The effect of locally induced flow structure on global heat transfer for plane laminar shear flow

M. Scholle, A. Haas, N. Aksel [a]
H.M. Thompson, R.W. Hewson, P.H. Gaskell [b]

[a] *Department of Applied Mechanics and Fluid Dynamics, University of Bayreuth, D–95440 Bayreuth, Germany.*

[b] *School of Mechanical Engineering, University of Leeds, Leeds, LS2 9JT, UK.*

Abstract

Heat transfer in a plane laminar shear flow configuration consisting of two infinitely long plates orientated parallel to each other is investigated theoretically. The upper plate, which is planar, drives the flow; the lower one, which is fixed, has a regular sinusoidally varying profile. A closed form analytical solution for velocity, based on lubrication theory, together with a semi–analytic one for temperature, from application of Ritz's direct method, is derived for creeping flow. In addition, detailed numerical solutions are obtained from a finite element formulation of the weak form of the governing equations for mass, momentum and energy (temperature) conservation, enabling the effects of inertia to be explored. It is shown that changes in the mean plate separation, that is the geometry, and the level of inertia present affect the local hydrodynamic flow structure in the form of kinematically and inertially induced eddies, respectively. These in turn impact on the local "laminar thermal mixing", and consequently enhance the global heat transfer. Results are reported for a wide range of Peclét, Reynolds and Nusselt numbers with agreement between the two methods of solution, for the case of creeping flow, found to be extremely good. The key flow features that emerge are:

(i) For creeping flow and varying Peclét number, the thermal field is asymmetric for all values of the Peclét number other than the limiting conditions of zero and infinity, at which extremes the corresponding thermal field is symmetric. In the limit of infinite Peclét number the eddy becomes a basin of fluid at uniform temperature.

(ii) Global heat transfer in the case of creeping flow, expressed in terms of the Nusselt number, for a given Peclét number increases as the mean plate separation decreases, that is as the local kinematically induced eddy structure becomes more pronounced.

(iii) There exists a subtle inter–play between variations in the mean plate separation and the level of inertia imposed, in that both influence the presence or otherwise of eddies. Starting from a creeping flow condition the introduction of inertia can in addition both enlarge and skew an existing eddy. When this information is condensed to a series of Nusselt number curves the indication is that it should be possible, from a practical standpoint, to find a critical mean plate separation, for a given Peclét number, for which local inertially influenced eddy effects on the global heat transfer are at a minimum.

Key words: Flow structure, thermal mixing, heat transfer, shear flow, topography
PACS: 44

---

1 Introduction

Simple laminar shear flow in a fluid confined between two rigid surfaces moving relative to one another remains of fundamental interest in fluid dynamics. With the case of Couette flow between two perfectly planar walls of infinite extent separated by a small distance and aligned parallel to each other and that of Taylor–Couette flow in the small gap formed between two concentrically aligned cylinders, being arguably the classical examples most often quoted. Even for this very small class of problems the associated literature is vast; for the interested reader the essential features are, however, adequately reported in most standard text books on fluid mechanics — see for example Tritton (1988), Panton (1996).

In practice, laminar shear flows arise across a broad swathe of engineering science where the confining surfaces involved are rarely completely parallel and/or they exhibit additional complicating features such as well defined irregularities in the form of sharp steps or trenches, or smoothly varying corrugations resulting from nature or as a consequence of a particular manufacturing process. The basis for the mathematical modelling of these and many other thin film flow problems remains the application of Reynolds' lubrication approximation, Reynolds (1886). In that, if the ratio of the cross–wise to stream–wise length scale is sufficiently small, the governing hydrodynamic equations reduce to a single equation, namely the Reynolds' equation, Spurk and Aksel (2008). It is possible to quote numerous such examples but the obvious ones encompass: the analysis of the load carrying capacity of thrust-bearings, journal bearings and gears, Dowson and Higginson (1966), Spurk and Aksel (2008), Szeri (1998), and associated thermal effects; the performance of replacement artificial joints, Jin et al. (2006); the stable operating windows of roll coating flows, (Kistler and Schweitzer (1997), Gaskell et al. (2001)).

The over arching problem of interest is that of laminar shear flow between

two horizontally aligned plates; the planar upper one moving with constant velocity and at a higher temperature than the lower one which is fixed and has a regular sinusoidally varying profile. Unlike Serifi et al. (2004), who consider the interplay between waves and heat transfer in free surface film flows, focus is directed at the interaction between eddies and heat transfer in Couette flows within the stable regime.

In the the case of isothermal laminar shear flows numerous examples exist were exploration of the effects of local flow structure on the global picture has proved extremely informative — see for example Gaskell et al. (1997), Wilson et al. (2005), Perry and Chang (1987), Jeffrey and Sherwood (1980), Scholle et al. (2006). What unifies all of these problems is that, even in the absence of inertia, the irregular confining geometry is a catalyst for eddy formation. Such a presence of eddies is of considerable practical interest in relation to the use of regular surface patterning to improve the performance of tribological components; since the onset of recirculating flow can significantly enhance load carrying capacity and reduce frictional drag in lubricated contacts, Sahlin et al. (2005), as well as reducing component wear due to wear debris becoming trapped in eddies, Etsion (2005). Of particular interest here is whether eddies – their size, shape and presence – enhance or otherwise the global heat transfer due to associated local "laminar thermal mixing"; not just in the creeping flow limit as the mean plate separation is varied but as inertia effects become important. Investigation of the current problem along such lines is motivated by the fact that in the case of creeping flow:

- it has been shown that a lower plate with a regular sinusoidally varying profile leads, under isothermal conditions, to kinematically induced eddies (Pozrikidis (1987), Scholle et al. (2004), Scholle (2004), Scholle (2007), Malevich et al. (2008)) as a consequence of the confining geometry;

- if the lower plate were flat as opposed to sinusoidally varying and at a temperature which is less than that of the planar upper one, the solution to this simple non–isothermal flow is trivial, White (2006). Convection is completely absent from the problem and the temperature field has a simple linear profile that is decoupled from the corresponding flow field which is devoid of eddies.

The problem as presented above is formulated in Section 2, followed by a description of the methods of solution in Section 3. The latter includes a comprehensive description of the semi–analytical approach adopted, based on lubrication theory and Ritz's direct method, for the case of creeping flow, and an outline of the finite element methodology used to solve the coupled set of governing equations of mass, momentum and energy (temperature) conservation enabling inertia effects to be investigated accurately. A corresponding comprehensive set of results is provided in Section 4 which includes, for creeping flow,

consideration of the temperature transition between the Peclét number limits of zero and infinity, thermal feedback in relation to "laminar thermal mixing" as a consequence of the underlying hydrodynamic flow structure as influenced by the mean plate separation, and hence the global heat transfer in the from of variation in the associated Nusselt number. The latter is also considered in detail from the standpoint of the additional influence of increasing inertia. Conclusions are drawn in Section 5.

2 Problem Formulation

Consider, as illustrated in Figure 1, the case of steady, two–dimensional Couette flow of an incompressible fluid confined between two infinite, horizontally aligned plates, with the moving upper flat plate, temperature T_0, separated by a small mean distance from the stationary lower one which has a regular sinusoidally varying profile and is at temperature T_1, ($T_1 > T_0$). The fluid properties are taken as those for silcon oil, as used Wierschem et al. (2003) in the investigation of the corresponding isothermal flow problem. Accordingly Tropea et al. (2007), Lide (1998), the thermal conductivity, λ, and specific heat, c_p, are assumed constant, while the mass density, ϱ, and viscosity, η have the form

$$\varrho\left(T\right) = \varrho_0\left[1 - \beta T\right] , \tag{1}$$
$$\eta\left(T\right) = \eta_0\left[1 - \eta^* T\right] , \tag{2}$$

with the non–dimensional constants β and η^* denoting the coefficients of thermal expansion and thermoviscosity, respectively.

2.1 Governing Equations

The corresponding governing equations for the velocity field, $\vec{u}$, the pressure, $\tilde{p}$, and the temperature field, $\tilde{T}$, are the continuity equation

$$\nabla \cdot \left[\varrho \vec{u}\right] = 0 , \tag{3}$$

the Navier–Stokes equations

$$\varrho\left(\vec{u} \cdot \nabla\right)\vec{u} = -\nabla\tilde{p} + \varrho\vec{g} + \nabla \cdot \left[2\eta\underline{\tilde{D}}\right] , \tag{4}$$

and temperature equation

$$\varrho c_p \left(\vec{u}\cdot\nabla\right)\tilde{T} - \nabla\cdot\left[\lambda\nabla\tilde{T}\right] = \tilde{\beta}\tilde{T}\left(\vec{u}\cdot\nabla\right)\tilde{p} + \tilde{\Phi}, \tag{5}$$

with

$$\underline{\tilde{D}} := \frac{1}{2}\left[\nabla\otimes\vec{u} + \left(\nabla\otimes\vec{u}\right)^T\right], \tag{6}$$

$$\tilde{\Phi} := 2\eta\,\mathrm{tr}\left(\underline{\tilde{D}}^2\right), \tag{7}$$

denoting the shear rate tensor and dissipation function, respectively.

With reference to Figure 1 the flow geometry is characterised by two non–dimensional parameters, namely the dimensionless mean plate separation, h, and amplitude, a of the lower plate; the coordinates x, z are scaled by $\Lambda/2\pi$, where Λ is the wavelength of the lower plate, and the corresponding velocity components by U, the velocity of the upper plate. If, in addition, the pressure and temperature are scaled as follows

$$\tilde{p} = 2\pi\eta_0\frac{U}{\Lambda}p\,; \qquad T := \frac{\tilde{T}-T_0}{T_1-T_0}\,, \qquad 1\le T\le 0, \tag{8}$$

the Navier–Stokes equations (4) take the following non–dimensional form

$$\begin{aligned}(1-\beta T)Re\left[u\frac{\partial u}{\partial x} + w\frac{\partial u}{\partial z}\right] &= -\frac{\partial p}{\partial x} + 2\frac{\partial}{\partial x}\left[(1-\eta^* T)\frac{\partial u}{\partial x}\right]\\ &\quad + \frac{\partial}{\partial z}\left[(1-\eta^* T)\left(\frac{\partial u}{\partial z} + \frac{\partial w}{\partial x}\right)\right], \end{aligned}\tag{9}$$

$$\begin{aligned}(1-\beta T)Re\left[u\frac{\partial w}{\partial x} + w\frac{\partial w}{\partial z}\right] &= -\frac{\partial p}{\partial z} + 2\frac{\partial}{\partial z}\left[(1-\eta^* T)\frac{\partial w}{\partial z}\right]\\ &\quad - \frac{Re}{Fr^2} + \frac{Re}{Fr^2}\beta T + \frac{\partial}{\partial x}\left[(1-\eta^* T)\left(\frac{\partial u}{\partial z} + \frac{\partial w}{\partial x}\right)\right], \end{aligned}\tag{10}$$

with the Reynolds number, Re, and Froude number, Fr, given by

$$Re := \frac{\varrho_0 U\Lambda}{2\pi\eta_0}\,, \qquad Fr := \sqrt{\frac{2\pi U^2}{g\Lambda}}\,, \tag{11}$$

respectively.

By taking Λ to be sufficiently small the system can be defined in such a way as to make Re arbitrarily small while Fr remains large. In such cases the combination $ReFr^{-2}$ becomes small and hence the buoyancy term, $ReFr^{-2}\beta T$, on

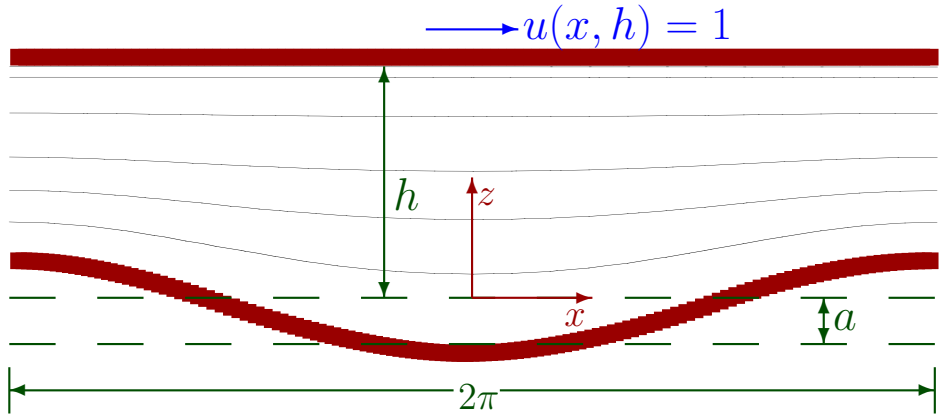

Fig. 1. Schematic of the flow geometry.

the right hand side of equation (10) can be neglected. With regard to stability against natural convection, if the buoyancy term is written alternatively as

$$\frac{Re}{Fr^2}\beta T = Ra\frac{8\pi^3\lambda U^3}{\varrho_0 c_p g^2 h^3 \Lambda^3}\,, \tag{12}$$

with the Rayleigh number, Ra, given by

$$Ra := \frac{\varrho^2 c_p g \beta h^3 \Lambda^3}{8\pi^3\eta\lambda}\,, \tag{13}$$

then, with a proper choice of parameters, Ra can be guaranteed to be below the critical stability limit of $Ra_c \approx 1700$ for natural convection, Chandrasekhar (1981).

Within the framework of the Boussinesq approximation the continuity equation (3) in non–dimensional form simplifies to

$$\frac{\partial u}{\partial x} + \frac{\partial w}{\partial z} = 0\,, \tag{14}$$

and with thermal expansion playing no part in the flow, terms involving βT can be neglected in the Navier–Stokes equations (9, 10) and in the temperature equation (5), reducing the latter to the following non–dimensional form

$$Pe\left[u\frac{\partial T}{\partial x} + w\frac{\partial T}{\partial z}\right] - \left[\frac{\partial^2 T}{\partial x^2} + \frac{\partial^2 T}{\partial z^2}\right] = PrEc\left[4\left(\frac{\partial u}{\partial x}\right)^2 + \left(\frac{\partial u}{\partial z} + \frac{\partial w}{\partial x}\right)^2\right], \tag{15}$$

with the Peclét, Eckert and the Prandtl numbers given, Spurk and Aksel (2008), by

$$Pe := \frac{\Lambda U \varrho_0 c_p}{2\pi\lambda}\,, \qquad Ec := \frac{U^2}{c_p(T_1 - T_0)}\,, \qquad Pr := \frac{c_p\eta}{\lambda}, \tag{16}$$

respectively.

The product $PrEc$ characterizes the ratio between dissipation and heat conduction. Accordingly, if $PrEc \ll 1$ dissipation can be assumed negligible and the term on the right hand side of equation (15) with $PrEc$ as a prefactor neglected, Spurk and Aksel (2008). For completeness, an estimation of the importance of heat production by dissipation is provided in Appendix B which supports this assumption.

Based on the above assumptions the full set of field equations underpinning the subsequent analyses reads:

$$\frac{\partial u}{\partial x} + \frac{\partial w}{\partial z} = 0, \tag{17}$$

$$-\frac{\partial p}{\partial x} + 2\frac{\partial}{\partial x}\left[(1-\eta^* T)\frac{\partial u}{\partial x}\right] + \frac{\partial}{\partial z}\left[(1-\eta^* T)\left(\frac{\partial u}{\partial z}+\frac{\partial w}{\partial x}\right)\right] = Re\left[u\frac{\partial u}{\partial x}+w\frac{\partial u}{\partial z}\right], \tag{18}$$

$$-\frac{\partial p}{\partial z} + 2\frac{\partial}{\partial z}\left[(1-\eta^* T)\frac{\partial w}{\partial z}\right] + \frac{\partial}{\partial x}\left[(1-\eta^* T)\left(\frac{\partial u}{\partial z}+\frac{\partial w}{\partial x}\right)\right] = Re\left[u\frac{\partial w}{\partial x}+w\frac{\partial w}{\partial z}\right], \tag{19}$$

$$Pe\left[u\frac{\partial T}{\partial x} + w\frac{\partial T}{\partial z}\right] - \left[\frac{\partial^2 T}{\partial x^2} + \frac{\partial^2 T}{\partial z^2}\right] = 0\,. \tag{20}$$

2.2 Boundary Conditions

In non–dimensional form the spatial locations of the lower and the upper plates are given by $z = -a\cos x$ and $z = h$, respectively, along which a no–slip condition is applied

$$u\,(x, -a\cos x) = 0, \tag{21}$$
$$w\,(x, -a\cos x) = 0, \tag{22}$$
$$u\,(x, h) = 1, \tag{23}$$
$$w\,(x, h) = 0. \tag{24}$$

For the temperature field the corresponding upper and lower plate conditions are the Dirichlet ones, namely

$$T\,(x, -a\cos x) = 1\,, \tag{25}$$
$$T\,(x, h) = 0\,. \tag{26}$$

The above are supplemented by periodic boundary conditions for all fields to the left and right of the flow domain.

3 Method of Solution

The equation set (17–20), which contains a full bilateral coupling between velocity, pressure and temperature is solved in one of two ways: semi–analytically in the limit of creeping flow; numerically for both creeping and finite Reynolds number flows.

3.1 Semi–analytical approach

As a means of simplification the problem is approached analytically by neglecting the thermoviscous coupling terms involving η^*, leading to the following unilaterally coupled (for velocity and pressure) set of equations for creeping flow, $Re \to 0$:

$$\frac{\partial u}{\partial x} + \frac{\partial w}{\partial z} = 0\,, \tag{27}$$

$$-\frac{\partial p}{\partial x} + \frac{\partial^2 u}{\partial x^2} + \frac{\partial^2 u}{\partial z^2} = 0\,, \tag{28}$$

$$-\frac{\partial p}{\partial z} + \frac{\partial^2 w}{\partial x^2} + \frac{\partial^2 w}{\partial z^2} = 0\,, \tag{29}$$

$$Pe\left[u\frac{\partial T}{\partial x} + w\frac{\partial T}{\partial z}\right] - \frac{\partial^2 T}{\partial x^2} - \frac{\partial^2 T}{\partial z^2} = 0\,, \tag{30}$$

enabling the hydrodynamic field to be solved separately from the temperature field, as described below.

3.1.1 Hydrodynamic field

Invoking the lubrication approximation, Spurk and Aksel (2008), reduces the hydrodynamic problem (27)–(29), to the Reynolds' equation, a single ordinary differential equation. Its closed form analytic solution Scholle (2004) ,Scholle (2007) leads to the following explicit expression for the streamfunction ψ,

$$\psi = hZ^2\left[\frac{h^2 - 4a^2 + 3a^2 Z}{2h^2 + a^2} + \frac{a}{h}(Z-1)\cos(x)\right]\,, \tag{31}$$

with

$$Z := \frac{z + a\cos x}{h + a\cos x}\,. \tag{32}$$

The corresponding velocity field is given by $u = \partial\psi/\partial z$ and $w = -\partial\psi/\partial x$.

3.1.2 Temperature field

Using the expression for Z given by (32) as a new coordinate, the lubrication solution (31) can be written as a non–orthogonal series expansion

$$\psi\,(x, Z) = \sum_{n=-1}^{+1} \psi_n\,(Z)\exp(-\mathrm{i}nx)\,, \tag{33}$$

with

$$\psi_0(Z) := \frac{h(h^2 - 4a^2)Z^2 + 3ha^2Z^3}{2h^2 + a^2}\,, \qquad \psi_{\pm1}(Z) := -\frac{a}{2}Z^2(1 - Z)\,. \tag{34}$$

The essence of the analysis is the construction of an analogous series representation for temperature, i.e.

$$T\,(x, Z) = \sum_{n=-M}^{+M} T_n\,(Z)\exp(-\mathrm{i}nx), \tag{35}$$

with $M \in \mathbb{N}$, and to determine the solution of the temperature equation (30) by means of a variational formulation as follows.

It is shown in Appendix A that equation (30) results from variation of the nonlocal functional

$$I := \int_{-\pi}^{+\pi}\int_{-a\cos x}^{h} \left[-Pe\,T(x,z)\,(\vec{u}\cdot\nabla)\,T(-x,z) + \nabla T(x,z)\cdot\nabla T(-x,z)\right]\mathrm{d}z\,\mathrm{d}x, \tag{36}$$

with respect to the temperature, provided that the velocity field is symmetric as per equations (A.6, A.7). For isothermal flow given by (31) these conditions are fulfilled. Use of the above variational formulation is advantageous since Ritz's direct method can be applied which represents an efficient means of solution.

After expressing ψ and T as truncated series via (33) and (35), substituting for Z according to (32) and integrating with respect to x, the functional (36) takes the form

$$I = 2\pi \int_0^1 L\left(T_k, T_k', Z\right) \mathrm{d}Z, \tag{37}$$

with 'Lagrangian'

$$\begin{aligned} L = & \sum_{n,m=-M}^{+M} T_n' \left[F_{n-m}\, T_m' + \mathrm{i}Pe\left(\psi_{n-m} + \psi_{m-n}\right) m T_m\right] \\ & + \sum_{m=-M}^{+M} m T_m \left\{ m h T_m + a\left[\frac{m+1}{2} T_{m+1} + \frac{m-1}{2} T_{m-1} - (1-Z)\left(T_{m+1}' - T_{m-1}'\right)\right]\right\}, \end{aligned} \tag{38}$$

where

$$F_k := \frac{(-A)^{|k|}}{\sqrt{h^2 - a^2}} + (1-Z)^2 \left[h\delta_{0k} - \frac{a}{2}\left(\delta_{1k} + \delta_{-1k}\right) - \sqrt{h^2 - a^2}\,(-A)^{|k|}\right], \tag{39}$$

$$A := \frac{a}{h + \sqrt{h^2 - a^2}}, \tag{40}$$

and $\psi_k = 0$ for $|k| \geq 2$.

Ritz's direct method proceeds by applying an approximation of the coefficient functions as linear combinations of $N \in \mathbb{N}$ independent basis functions $\varphi_k(Z)$ according to

$$T_n(Z) = T_{inh,n}(Z) + \sum_{n=1}^{N} T_{nk}\varphi_k(Z), \tag{41}$$

with $\varphi_k(0) = \varphi_k(1) = 0$ and arbitrary functions $T_{inh,n}(Z)$ fulfilling the boundary conditions. In the present case the boundary conditions

$$T_n(0) = \delta_{0n}, \tag{42}$$

$$T_n(1) = 0, \tag{43}$$

of Dirichlet–type, result from expressions (25) and (26) and the form of (35); by virtue of the fact that

$$T_{inh,n}(Z) = (1-Z)\delta_{0n}, \tag{44}$$

the boundary conditions are indeed fulfilled. For $\varphi_k(Z)$ a set of functions are chosen which allow for a proper approximation of arbitrary steady functions on the interval $[0, 1]$ with vanishing values at the boundaries. We make use of linear combinations of shifted Chebyshev polynomials fulfilling the requirement that $\varphi_k(0) = \varphi_k(1) = 0$, the main reason being that these allow for fast calculation when computer algebra Maple (2006) is used. Proceeding in this way results in a quadratic expression for the coefficients T_{nk}. Finally, variation with respect to T_{nk} produces a linear algebraic set of equations for the coefficients T_{nk} which is again solved within MAPLE.

3.2 Finite element approach

The weak form of equations (17) to (20) were solved numerically using the commercially available finite element package, COMSOL (2005). The finite element method as a means of solving incompressible fluid flow problems is well established and as such much of the underlying detail can be omitted — see for example Zienkiewicz et al. (2005). Suffice it to say a non-uniform mesh comprised of triangular elements clustered towards the lower plate was used to discretise the flow domain, employing second order interpolation functions for velocities and temperature and first order interpolation for pressure. The resulting system of equations was solved iteratively using a form of the damped Newton method as described in Deuflhar (1974). The problem was programmed in the MATLAB environment to allow for the flexible control of geometric and fluid parameters.

A variety of mesh densities was examined to establish the number and distribution of elements required to guarantee mesh independent solutions for the parameter range investigated. For a typical flow geometry with $a = 1/2$ and $h = 3/4$ the number of elements required to ensure mesh independence was found to be 275710.

4 Results and Discussion

Results for creeping flow and flow with inertia are presented independently of each other.

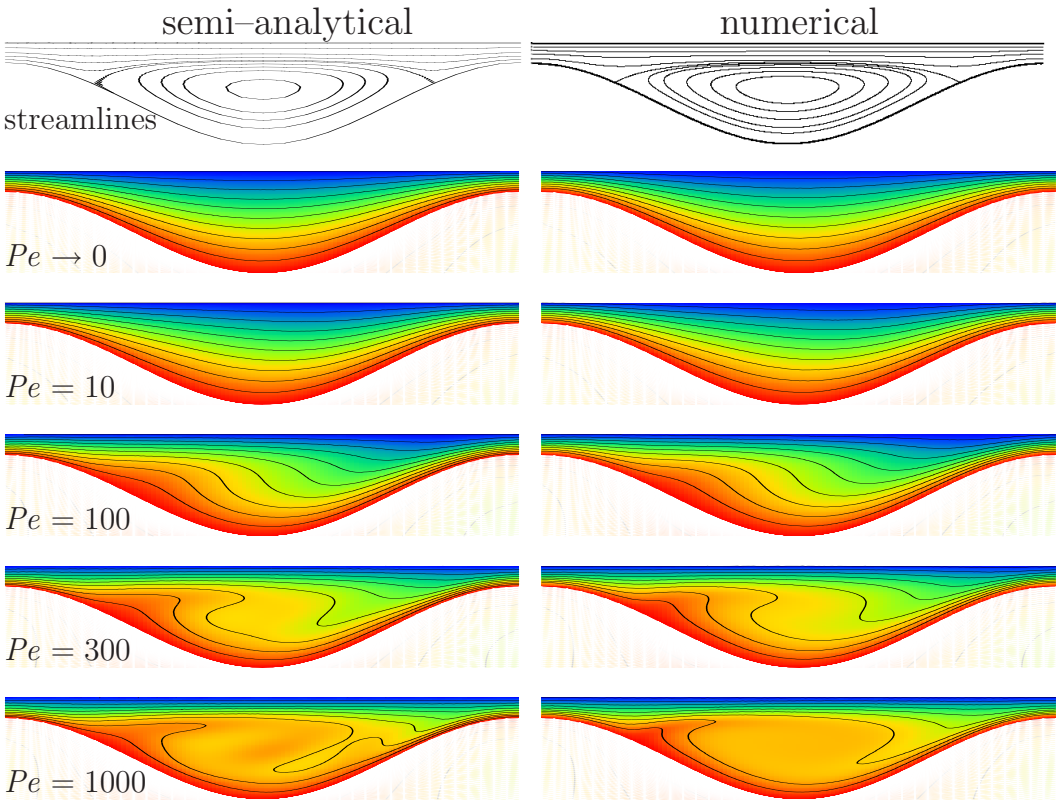

Fig. 2. Flow structure (streamlines) and corresponding temperature field (isotherms) transition with increasing Pe, obtained semi–analytically (left) and numerically (right), for the case $a = 1/2$, $h = 3/4$.

4.1 Creeping Flow

4.1.1 Temperature field transition

Representative results for the transition experienced by the temperature field with increasing Peclét number are presented, see Figure 2, for the case $a = 1/2$ and a mean plate separation of $h = 3/4$. These were obtained: (i) using the semi–analytical approach, with $M = 4$ modes for the series (35) and $N = 2 \cdot 4 + 1 = 9$ for the expansion (41); (ii) numerically as described above.

Agreement between the two sets of results is seen to be remarkably close, with the streamline plots showing that the geometry as specified results in the presence of a large symmetric eddy while the nature of the corresponding temperature field is Peclét number dependent. When $Pe \to 0$ the problem is one of pure heat conduction and the temperature field is symmetric as shown. Symmetry is, however, soon lost due to the presence of convection as demonstrated for the case $Pe = 10$. As Pe, is increased further a point is soon reached, when for sufficiently large values, see for example the case $Pe = 100$, the asymmetry present becomes pronounced as warmer fluid is transported

upwards on the left side of the domain with a corresponding downward movement of colder fluid on the right. For Peclét numbers of approximately 300 and greater, the isotherms mimick the corresponding streamline pattern with "laminar thermal mixing" occurring.

4.1.2 Temperature field limit cases

Consider the limit case of very large Peclét numbers, that is $Pe \to \infty$. Although this rules out completely the possibility of obtaining a numerical solution to equations (17)–(20) while the semi–analytic solution to equation (30) becomes singular at this limit, it is possible to explore the limit case analytically, since at $Pe \to \infty$ equation (30) degenerates to the following first order PDE:

$$\frac{\partial \psi}{\partial z}\frac{\partial T}{\partial x} - \frac{\partial \psi}{\partial x}\frac{\partial T}{\partial z} = 0\,, \tag{45}$$

having the general solution

$$T = F\left(\psi\right)\,, \tag{46}$$

with an unknown function F, and with the predicted isotherms considered identical to the predicted streamlines. However, the associated boundary conditions $T\left(x, -a\cos x\right) = 1$, $T\left(x, h\right) = 0$ do not allow for the direct determination of the unknown function F.

Alternatively, a reasonable approximation for the function F in (46) can be obtained by considering the case when both upper and lower plates are planer, that is $a = 0$, for which streamfunction and temperature field are given by the closed analytic expressions

$$\psi = \frac{z^2}{2h} = \frac{h}{2}Z^2\,, \tag{47}$$

$$T = 1 - \frac{z}{h} = 1 - Z\,, \tag{48}$$

respectively. By eliminating the coordinate Z, the following relationship

$$T = 1 - \sqrt{\frac{\psi}{\psi_s}}\,, \tag{49}$$

between streamfunction and temperature results, where $\psi_s := \psi(x, h)$ denotes the value of the streamfunction at the upper plate. Since equation (49) is valid

for arbitrary Peclét number, it holds for the temperature field when $Pe \to \infty$ for the case $a = 0$.

If it is further assumed that F, in a general sense, is only weakly dependent on a (and h) it is reasonable to expect that (49) will remain valid in the limit $Pe \to \infty$ for $a > 0$, at least within that part of the flow region with $\psi \geq 0$, that is outside the core of any eddy present. Inside such an eddy the streamlines and therefore the isotherms are closed, with thermodynamical equilibrium requiring a constant temperature inside the eddy. Since such eddies are in contact with the lower plate, this constant temperature is $T = 1$.

Summarizing the above considerations as

$$T_\infty \approx \left\{ \begin{matrix} 1 - \sqrt{\frac{\psi}{\psi_s}} \ , \ \psi \geq 0 \\ 1 \qquad\qquad , \ \psi < 0 \end{matrix} \right\} = 1 - \Re\sqrt{\frac{\psi}{\psi_s}}, \tag{50}$$

a good approximation for the temperature field exists where $\Re$ denotes the real part of a complex number. Using the explicit form (31) of the streamfunction leads to

$$T_\infty \approx 1 - Z\Re\sqrt{1 - \frac{3ha^2 + a\,(2h^2 + a^2)\cos x}{h\,(h^2 - a^2)}(1 - Z)}, \tag{51}$$

as an appropriate analytic approximation for the temperature field at very large Peclét numbers.

Figure 3 depicts the temperature field and associated streamline pattern, that is flow structure, when $a = 1/2$, $h = 1$, for the two limit cases. The solution of equation (51) for the limit case $Pe \to \infty$, Figure 3b, shows that: outside of the eddy the temperature field and streamlines follow each other; within the eddy a basin of fluid at a uniform temperature equal to that of the lower plate is formed. Note that the same flow and temperature field is established irrespective of whether the upper plate is hotter than the lower one or vice versa. Contrasting this with the solution of Figure 3a, for the limiting case of pure heat conduction when $Pe \to 0$, it can be seen that at this extreme the temperture field and steamlines do not follow each other, and that in particular within the eddy itself the streamlines cross different values of the temperature field.

An interesting feature of the temperature field in terms of the Pe is the symmetry it exhibits at both extremes, while for any finite Pe it is asymmetric, which can be explained as follows. For $Pe \to 0$ and $Pe \to \infty$ equation (30) simplifies to the Laplace equation having even parity and equation (45) having

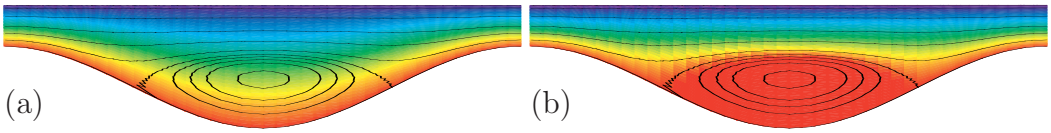

Fig. 3. Flow structure (streamlines) and corresponding temperature field for the limit cases (a) $Pe \to 0$ and (b) $Pe \to \infty$, when $a = 1/2$, $h = 1$.

odd parity, respectively, with respect to the operation $x \to -x$. In contrast to this, equation (30) has broken parity for any finite Pe which, therefore, always leads to an asymmetric temperature field.

The above considerations imply that a maximum asymmetry must arise at a specific value of the Peclét number, an adequate quantitative measure of which can be determined with reference to the series representation (35), which can be written alternatively as

$$T\left(x,Z\right) = T_0\left(Z\right) + 2\sum_{n=1}^{M}\left[\Re T_n\left(Z\right)\cos(nx) + \Im T_n\left(Z\right)\sin(nx)\right]\,, \tag{52}$$

where $\Re$ and $\Im$ denote real and imaginary parts. In the above $\Im T_1(Z)\sin x$ appears as the leading term which is responsible for the asymmetry, the imaginary part of which provides a quantitative means of measuring the asymmetry. For a flow geometry defined by $h = 3/4$ and $a = 1/2$, the asymmetry reaches a maximum at a $Pe \approx 100$.

4.1.3 Global heat transport

A measure for the global heat transport is provided by the Nusselt number Nu which is found from the temperature field as

$$Nu = -\frac{h}{2\pi}\int_{-\pi}^{+\pi}\left.\frac{\partial T}{\partial z}\right|_{z=h}\mathrm{d}x\,. \tag{53}$$

It represents the non–dimensional global heat flux, scaled with the corresponding heat flux $\lambda(T_1 - T_0)/h$ for Couette flow between parallel flat plates fixed at the same reference temperatures and in which case $Nu = 1$. In terms of the semi–analytical approach described in Section 3.1, the series representation (35) for the temperature can be inserted into expression (53) directly, such that Nusselt number is given by

$$Nu = -\frac{h}{2\pi}\int_{-\pi}^{+\pi}\sum_{n=-M}^{+M} T_n'\left(1\right)\frac{\exp(-\mathrm{i}nx)}{h + a\cos x}\mathrm{d}x \tag{54}$$

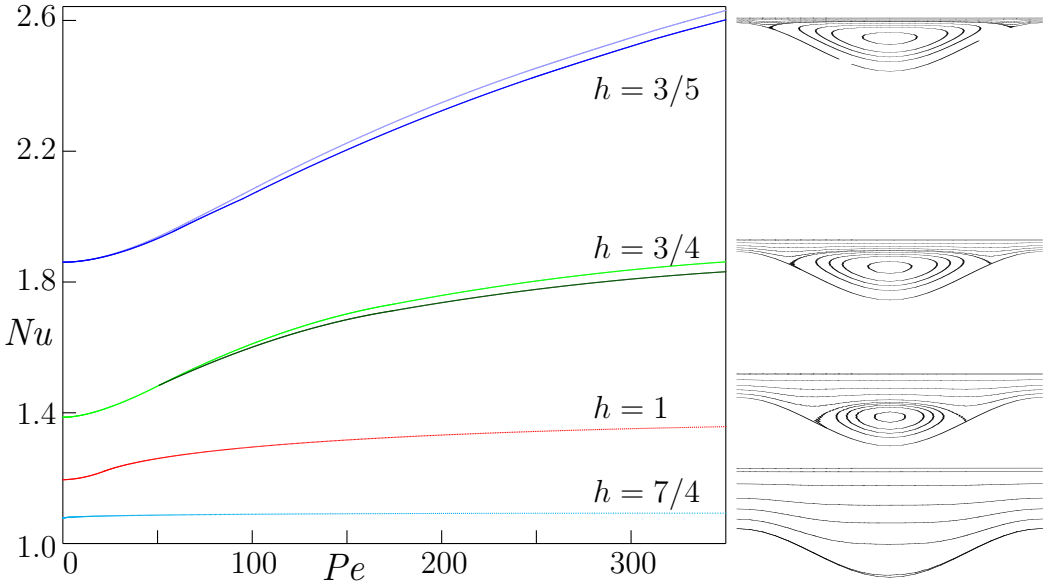

Fig. 4. Global heat transport depicted as plots of Nusselt number vs. Peclét number for the case of a lower plate with amplitude $a = 1/2$ and four different mean plate separations. For $h = 3/5$ and $h = 3/4$ the upper curves represent those obtained semi–analytical ($M = 3$, $N = 14$), the lower ones those obtained numerically. For $h = 1$ and $h = 7/4$ both sets of results are indistinguishable. The streamline plots to the right show the underlying flow structure in each case.

$$= - \sum_{n=-M}^{+M} T_n'(1) \frac{h}{2\pi} \int_{-\pi}^{+\pi} \frac{\exp(-\mathrm{i}nx)}{h + a\cos x} \mathrm{d}x = -h \sum_{n=-M}^{+M} \frac{(-A)^{|n|} T_n'(1)}{\sqrt{h^2 - a^2}} .$$

The Nusselt number was calculated both semi–analytically and numerically for the case of a bottom plate with amplitude $a = 1/2$ and for different mean plate separations, the results of which are plotted against Peclét number in Figure 4. Values of h were chosen in such a way that four qualitatively different cases could be investigated: one without an eddy present ($h = 7/4$), a second exhibiting a small eddy ($h = 1$), the third with a large eddy present ($h = 3/4$), and a forth case in which the flow has all but degenerated to that of a driven–cavity like flow consisting almost entirely of a large single eddy ($h = 3/5$). In all cases the analytical and numerical results are in very good agreement with each other.

Compared to the case of parallel plates ($Nu = 1$), it can be seen that there is already an improvement in the global heat transport for $Pe \to 0$; that is, even in the case of pure heat conduction it is observed that $Nu > 1$ as a consequence of the geometry. This purely geometric effect can be estimated from a simple one–dimensional model for conduction assuming that the direction of the heat flux is nearly vertical, which is justifiable especially for small amplitudes, a. This leads to a local Nusselt number of the form $h/(h + a\cos x)$ and therefore

to a global one according to

$$Nu(0) \approx \frac{h}{2\pi} \int_{-\pi}^{+\pi} \frac{\mathrm{d}x}{h + a\cos x} = \frac{1}{\sqrt{1 - \left(\frac{a}{h}\right)^2}} \tag{55}$$

According to Table 1, which draws comparisons to exact values of $Nu(0)$, the above simple formula (55) delivers a reasonable estimate of the enhancement of heat transport due to geometry for the moderate amplitude case, $a = 1/2$, considered.

mean plate separation h	7/4	1	3/4	3/5
$Nu(0)$, 1D model	1.043	1.155	1.342	1.809
$Nu(0)$, exact	1.076	1.190	1.376	1.837

Table 1
Comparison of Nusselt number predictions, exact vs. one-dimensional conduction model results, for different mean plate separations in the limit $Pe \to 0$, for the case $a = 1/2$.

For $Pe > 0$ an additional increase in Nu, due to convection, is apparent. This effect, however, depends significantly on the eddy size: for the case $h = 7/4$, one without an eddy, only a tiny improvement in the heat flux is observed, whereas the curve corresponding to the flow containing a small eddy ($h = 1$) reveals a distinct gradual increase of the Nusselt number with increasing Pe. This effect becomes even more pronounced the larger the eddy ($h = 3/4$) and especially so in the case of a driven–cavity like flow ($h = 3/5$). In order to separate out the eddy effect from that of the geometry it is useful to consider a kind of "weighted Nusselt number", $Nu(Pe)/Nu(0)$, by which the enhancement of heat transport relative to that of heat transport due to pure conduction is given. The corresponding plots are shown in Figure 5.

In order to estimate the upper limit of the four monotonically increasing curves shown in Figure 4, the asymptotic case $Pe \to \infty$ is also considered by calculating the Nusselt numbers corresponding to the approximation for the temperature field for very large Peclét numbers discussed above: the analytic approximation (51) leads, according to (53), to the simple expression

$$Nu_\infty \approx \frac{2h^2 + a^2}{2(h^2 - a^2)}. \tag{56}$$

Results, corresponding to the same four geometries as in Figure 4, are provided in Table 2.

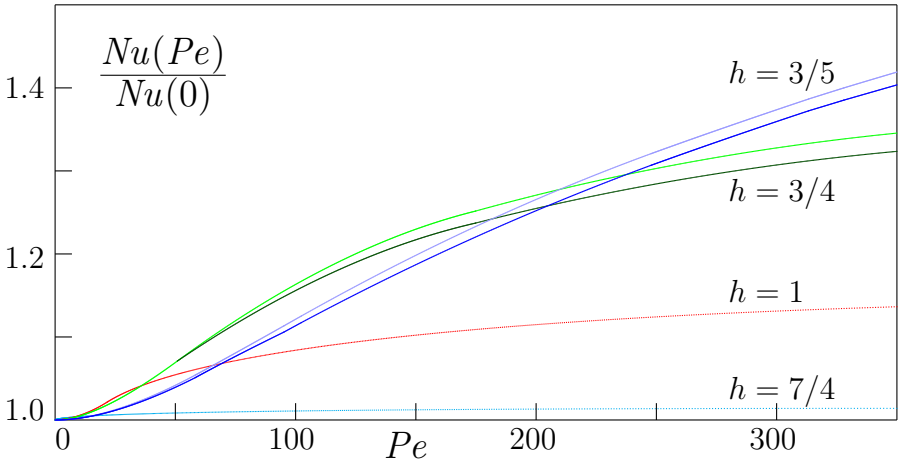

Fig. 5. Weighted Nusselt number $Nu(Pe)/Nu(0)$ vs. Peclét number as per Fig. 4.

mean plate separation h	7/4	1	3/4	3/5
$Nu(\infty)$	1.13	1.50	2.20	4.41

Table 2
Analytically obtained Nusselt numbers for different mean plate separations in the limit $Pe \to \infty$, when $a = 1/2$.

4.1.4 Thermal feedback to the flow

Thermal feedback due to thermoviscosity $\eta = \eta(T)$ is investigated numerically, with buoyancy and thermal expansion effects due to $\varrho = \varrho(T)$ neglected, as discussed in Section 2.1.

In Figure 6 results are shown for the case $a = 1/2$, $h = 3/4$, a Peclét number $Pe = 100$ and a thermoviscous coupling with $\eta^* = 1/3$ corresponding to a temperature–dependent viscosity given by

$$\eta(T) = \eta_0 \left[1 - \frac{T}{3}\right] . \tag{57}$$

Note that this choice of temperature dependence leads to a fluid viscosity that is 50% larger at the colder plate than at the warmer one. Hence, a strong thermoviscous coupling is implicit in the calculations. For comparison purposes streamlines and isotherms are shown for the case of constant viscosity. Shown also is the constant viscosity case when the temperatures of the plates are reversed — that is, the top plate is hotter than the bottom one.

The surprising result which emerges from this figure is that, even in the case of strong thermoviscous coupling, the feedback effect of the temperature on the flow is negligibly small. Moreover, by comparing the resulting temperature fields there is no discernible difference, even in the case when the temperatures of the upper and lower plates are reversed. Accordingly, this result supports

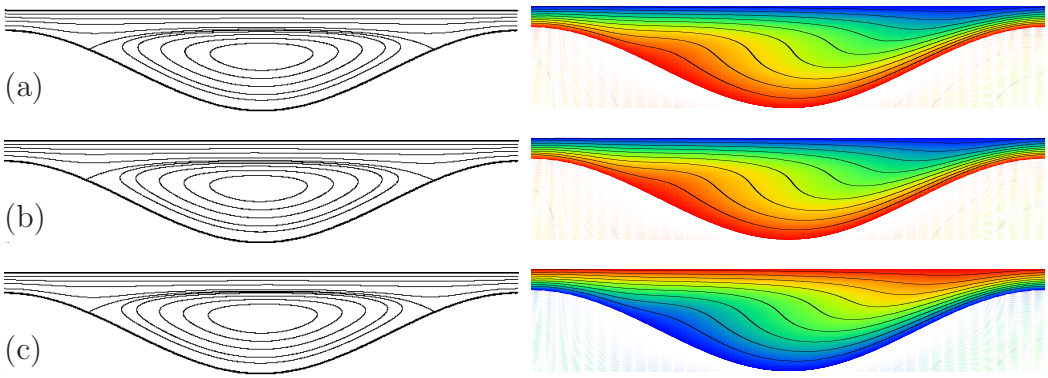

Fig. 6. Numerically calculated streamlines (left) and corresponding isotherms (right) for a flow geometry with $a = 1/2$ and $h = 3/4$, and $Pe = 100$: (a) constant viscosity; (b) viscosity according to equation (57); (c) as (a) but with the upper and lower plate temperatures reversed.

the *a priori* assumption made when formulating the semi–analytical method of solution that the flow and temperature fields can be decoupled.

4.2 Flow with finite Reynolds number

4.2.1 Effect of increasing inertia

Numerical solutions were obtained, see Figure 7, for Stokes flow and at Reynolds number $Re = 100$ for the case $a = 1/2$ and the same four mean plate separations as considered in Figure 4, and with $Pe = 100$. The streamline plots to the left, for Stokes flow, show the influence of the mean plate separation, that is the geometry, on the eddy structure present; those on the right, for the case $Re = 100$, reveal that the presence of inertia can lead to both eddy generation and to increased asymmetry of an existing eddy structure. The shift in the vortex core, in the case of the latter, has consequences for the corresponding temperature field: in that the area where the heat transport due to convection is significant is also shifted to the right.

4.2.2 Global heat transport

Using equation (53) the Nusselt number was calculated for the case of a lower plate with amplitude $a = 1/2$, for the same four mean plate separations. This was done at three different Reynolds numbers $Re = 10$, 100, 300 for Peclét numbers between 0 and 350. The resulting curves of Nu versus Pe are shown in Figure 8. Compare these with those in Figure 4 for the corresponding creeping flow problem.

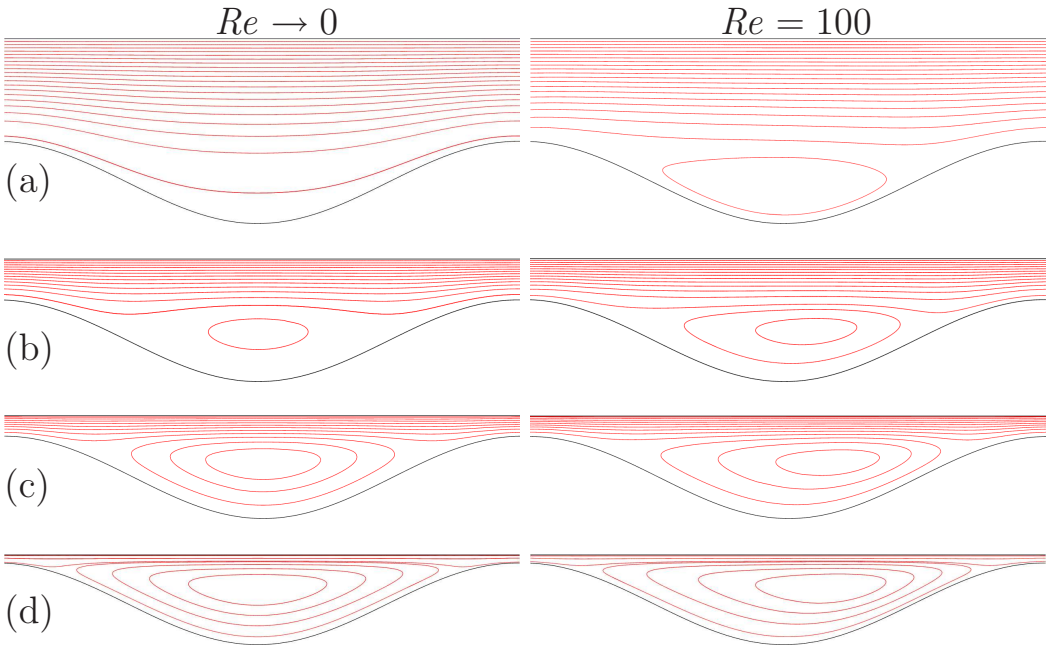

Fig. 7. Comparison of streamline plots of the flow structure for the case of a lower plate with amplitude $a = 1/2$, and mean plate separations of: (a) $h = 7/4$; (b) $h = 1$; (c) $h = 3/4$; (d) $h = 3/5$; $Pe = 100$. Creeping flow conditions (left); Reynolds number 100 (right).

The effect of inertia is qualitatively different for the four geometries considered: in the two cases (d) and (c) commensurate with a smaller mean plate separation, $h = 3/5$ and $h = 3/4$ respectively, the global heat transport is reduced with increasing inertia, whereas in the two cases (b) and (a) with a larger mean plate separation, $h = 1$ and $h = 7/4$ respectively, the opposite occurs and it is enhanced. The explanation for this qualitative difference is found by examining the underlying flow structures. In the case $h = 3/4$, for instance, the corresponding velocity field shown in Figure 7 reveals a shift to the right of the vortex core. Therefore, the area over which convective heat transport is relevant is reduced. The same qualitative effect is found for $h = 3/5$, since in this case too there is a large eddy in the flow. In contrast, for $h = 1$ there is only a small eddy present, while for $h = 7/4$ there is no eddy present at all in the creeping flow case. In the latter two cases an existing eddy is enlarged and eddy is created, respectively, due to inertia, assisting the transport of heat which shows as a corresponding increase in the Nusselt number.

Consequently, there should be a geometry $a = 1/2$, $h = h_c$ with a critical mean plate distance h_c for which the competing interplay between kinetic and inertially induced eddy effects cancel each other out, such that a curve results which is relatively insensitive to Reynolds number effects.

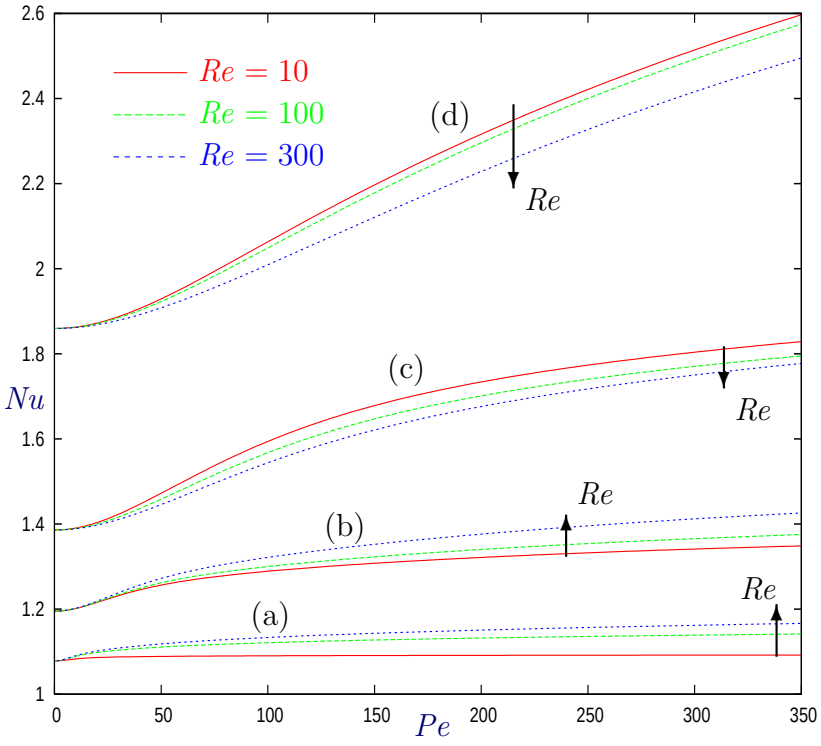

Fig. 8. Global heat transport depicted as plots of Nusselt number vs. Peclét number, at three different Reynolds numbers, for a lower plate with amplitude $a = 1/2$ and the four mean plate separations (a)–(d) used in Figure 7.

5 Conclusions

The subtle interplay that exists between the global transfer of heat and the underlying flow structure and hence local "laminar thermal mixing" in the case of shear flow between two rigid surfaces at different fixed temperatures — the hot, upper one, planar; the lower, cooler one, varying sinusoidally — a small mean distance apart, has been explored both analytically and numerically.

For creeping flow conditions and varying Peclét number, the thermal field is found to be asymmetric for all values of the Peclét number other than the limiting conditions of zero and infinity, at which extremes the corresponding thermal field is symmetric. The latter limiting condition ($Pe \rightarrow \infty$) is of particular note since in this case the isotherms representing the temperature field and streamlines depicting the underlying flow structure are found to follow each other, with the additional feature that within an eddy a basin of fluid at a uniform temperature equal to that of the lower plate is established. This feature has interesting possibilities in relation to using local, surface–contour dependent thermal mixing to control and establish basins of constant temperature for fixed thermal boundary conditions. Examples of where this type of global flow structure could prove usefull is for the: trapping of living organisms in basins of constant temperature over a large surface area for

use as local incubators before releasing the organisms again into the main flow; cooling of neutrally buoyant micro- and nano–particles as one stage in a particular process.

Global heat transport, in the form of plots of Nusselt number against Peclét number, is investigated with agreement between predictions from analysis and ones obtained numerically seen to be extremely good, particularly for higher values of mean plate separation. It is found that compared to the case when both top and bottom plates are flat there is an improvement to be seen in global heat transport as a consequence of the geometry, even for the case of pure heat conduction ($Pe \to 0$), but which depends significantly on the size of the underlying eddy structure present as the Peclét number is increased and convection plays a more significant role. In addition, the case $Pe \to 0$ lends itself conveniently to a simple one-dimensional analysis of heat conduction, enabling a reasonable estimate of global heat transport due to geometry alone to be obtained. For completeness, a simple analytical expression in terms of the amplitude of the lower plate and mean plate separation is derived to determine the Nusselt number limit as the Peclét number tends to infinity.

In the case of non–creeping flow, the effect of increasing inertia on both the temperature field and global heat transport is revealed, the obvious one being to skew the underlying eddy structure — for moderate Reynolds numbers, $Re = 100$, this takes the form of a shift to the right of the vortex core. The consequence for the corresponding temperature fields is that the region where heat transfer due to convection is significant is also skewed in the same direction. The results obtained for global heat transfer expose the interrelationship between eddies induced kinematically and due to inertia, in that inertia can result in the creation of an eddy or enlarge an existing eddy, for a given lower plate profile and mean plate separation, that is fixed flow geometry. Indeed the present work suggests that for a given sinusoidal variation of the lower plate it should be possible, from a practical standpoint, to find a critical mean plate separation for which Reynolds number effects on the global heat transfer are minimised.

Acknowledgement

Professor N Aksel wishes to thank the EPSRC for the provision of Visiting Fellowship, Grant No. EP/E029183., which made this collaboration possible.

Appendices

A Variational formulation for heat conduction with convection

The equation for heat conduction with convection is a parabolic PDE and therefore not self–adjoint. For heat conduction in a rigid body Anthony (2001) proposes a variational formulation which in terms of non–dimensional quantities reads

$$I_1 = \int_{t_1}^{t_2} \int_A \{-Pe\, T \partial_t[\varphi - \varphi_0(T,t)] + \nabla[\varphi - \varphi_0(T,t)] \cdot \nabla T\} \,\mathrm{d}x \,\mathrm{d}z \,\mathrm{d}t\,, \quad \text{(A.1)}$$

for two–dimensional problems, that is $T = T(x,z,t)$ and $\varphi = \varphi(x,z,t)$, with A denoting the area of the system. An additional total time derivative has been neglected in the integrand.

For steady flows, equation (A.1) is modified by replacing the time derivative ∂_t by the material time derivative $\vec{u} \cdot \nabla$, substituting $\tilde{\varphi} := \varphi - \varphi_0(T,t)$ and skipping the integration with respect to time. Then free variation of the functional

$$I_2 = \int_A \{-Pe\, T \vec{u} \cdot \nabla \tilde{\varphi} + \nabla \tilde{\varphi} \cdot \nabla T\} \,\mathrm{d}x \,\mathrm{d}z\,, \quad \text{(A.2)}$$

with respect to $\tilde{\varphi}$ yields the heat conduction equation with convection

$$Pe\, (\vec{u} \cdot \nabla)\, T - \Delta T = 0\ ; \quad \text{(A.3)}$$

whereas variation with respect to T yields

$$-Pe\, (\vec{u} \cdot \nabla)\, \tilde{\varphi} - \Delta \tilde{\varphi} = 0\,, \quad \text{(A.4)}$$

as the field equation for $\tilde{\varphi}$. The meaning of the additional field $\tilde{\varphi}$ is not obvious. Anthony (2001), interprets (A.1) as the truncated part of an extended action functional which takes non–equilibrium aspects of thermodynamics into account. In this context $\tilde{\varphi}$ becomes a measure for the deviation from local equilibrium.

An alternative approach is motivated by the early work of Bateman (1931). By finding a non–vanishing particular solution of (A.4) and inserting this solution in the functional (A.2), the additional field $\tilde{\varphi}$ can be eliminated following the line of Sievers and Anthony (1996) as follows.

The parity operator $\hat{\mathrm{P}}$ is introduced which substitutes x for $-x$. Then, considering the symmetry of the velocity field $\vec{u}$, by

$$\tilde{\varphi}(x,z) = \hat{\mathrm{P}}T(x,z) = T(-x,z) \tag{A.5}$$

a non–trivial particular solution of (A.4) is given, provided that the velocity field is symmetric, i.e

$$\hat{\mathrm{P}}u = u\,, \tag{A.6}$$
$$\hat{\mathrm{P}}w = -w\,. \tag{A.7}$$

Hence, the functional (A.2) results in the nonlocal form

$$I = \int\limits_A \left\{ -Pe\, T(\vec{u}\cdot\nabla)\hat{\mathrm{P}}T + \nabla T\cdot\nabla\hat{\mathrm{P}}T \right\} \mathrm{d}x\,\mathrm{d}z\,, \tag{A.8}$$

which for the geometry of interest here results in (36). The temperature T enters the functional (A.8) as the only field to be varied. Note that the velocity field $\vec{u}$ is a control parameter. Variation

$$T(x,z) \to T(x,z) + \delta T(x,z) \tag{A.9}$$

of the temperature with $\delta T = 0$ for $(x,z) \in \partial A$ gives:

$$\begin{aligned}
\delta I = &\int\limits_A \left[-Pe(T+\delta T)(\vec{u}\cdot\nabla)\hat{\mathrm{P}}(T+\delta T) + \nabla(T+\delta T)\cdot\nabla\hat{\mathrm{P}}(T+\delta T) \right] \mathrm{d}x\,\mathrm{d}z \\
&- \int\limits_A \left[-Pe\, T(\vec{u}\cdot\nabla)\hat{\mathrm{P}}T + \nabla T\cdot\nabla\hat{\mathrm{P}}T \right] \mathrm{d}x\,\mathrm{d}z\,, \\
= &\int\limits_A \left[-Pe\,\delta T(\vec{u}\cdot\nabla)\hat{\mathrm{P}}T + \nabla\delta T\cdot\nabla\hat{\mathrm{P}}T \right] \mathrm{d}x\,\mathrm{d}z \\
&+ \int\limits_A \left[-Pe\, T(\vec{u}\cdot\nabla)\hat{\mathrm{P}}\delta T + \nabla T\cdot\nabla\hat{\mathrm{P}}\delta T \right] \mathrm{d}x\,\mathrm{d}z + \mathcal{O}(\delta T^2)\,.
\end{aligned}$$

By considering $\hat{\mathrm{P}}^2 T = T$, $\partial_x\hat{\mathrm{P}}T = -\hat{\mathrm{P}}\partial_x T$, $\partial_z\hat{\mathrm{P}}T = \hat{\mathrm{P}}\partial_z T$ and

$$\int\limits_A [\cdots]\,\mathrm{d}x\,\mathrm{d}z = -\int\limits_{\hat{\mathrm{P}}A} \hat{\mathrm{P}}\,[\cdots]\,\mathrm{d}x\,\mathrm{d}z = +\int\limits_A \hat{\mathrm{P}}\,[\cdots]\,\mathrm{d}x\,\mathrm{d}z\,,$$

the first integral in the above formula can be transformed into

$$\int_A \left[-Pe\,\delta T(\vec{u}\cdot\nabla)\hat{\mathrm{P}}T + \nabla\delta T\cdot\nabla\hat{\mathrm{P}}T\right]\mathrm{d}x\,\mathrm{d}z$$
$$= \int_A \left[+Pe\,\hat{\mathrm{P}}\delta T(\vec{u}\cdot\nabla)T + \nabla\hat{\mathrm{P}}\delta T\cdot\nabla T\right]\mathrm{d}x\,\mathrm{d}z\,,$$

and hence, considering that δT vanishes on the boundary ∂A, the variation of the functional (A.8) reads

$$\begin{aligned}\delta I &= \int_A \left[Pe\left(\hat{\mathrm{P}}\delta T(\vec{u}\cdot\nabla)T - T(\vec{u}\cdot\nabla)\hat{\mathrm{P}}\delta T\right) + 2\nabla T\cdot\nabla\hat{\mathrm{P}}\delta T\right]\mathrm{d}x\,\mathrm{d}z + \mathcal{O}(\delta T^2)\,,\\ &= 2\int_A \hat{\mathrm{P}}\delta T\left[Pe\,(\vec{u}\cdot\nabla)\,T - \Delta T\right]\mathrm{d}x\,\mathrm{d}z + \int_{\partial A}\hat{\mathrm{P}}\delta T\left[\nabla T - Pe\,T\vec{u}\right]\cdot\vec{n}\mathrm{d}S + \mathcal{O}(\delta T^2)\,,\\ &= 2\int_A \hat{\mathrm{P}}\delta T\left[Pe\,(\vec{u}\cdot\nabla)\,T - \Delta T\right]\mathrm{d}x\,\mathrm{d}z + \mathcal{O}(\delta T^2)\,.\end{aligned}$$

Since the variation of the temperature is for arbitrary δT, the above equation finally yields the field equation (A.3) for conduction with convection.

B Heat production by dissipation

The effect of heat production by dissipation according to the right hand side of the temperature equation (15) is considered. Since this equation is linear, the effect can be treated separately without considering the heat transfer imposed by a temperature difference between the two plates. It is therefore convenient to make use of the rescaling

$$T^* := \frac{T}{PrEc} = \frac{\lambda\left(\tilde{T} - T_0\right)}{\eta_0 U^2}\,, \tag{B.1}$$

in order to eliminate the dimensionless parameter $PrEc$ from the problem. Equation (15) then reads

$$Pe\left[u\frac{\partial T^*}{\partial x} + w\frac{\partial T^*}{\partial z}\right] - \left[\frac{\partial^2 T^*}{\partial x^2} + \frac{\partial^2 T^*}{\partial z^2}\right] = 4\left(\frac{\partial u}{\partial x}\right)^2 + \left(\frac{\partial u}{\partial z} + \frac{\partial w}{\partial x}\right)^2. \tag{B.2}$$

This field equation is subject to the following Dirichlet boundary conditions

$$T\left(x, -a\cos x\right) = 0\,, \tag{B.3}$$
$$T\left(x, h\right) = 0\,, \tag{B.4}$$

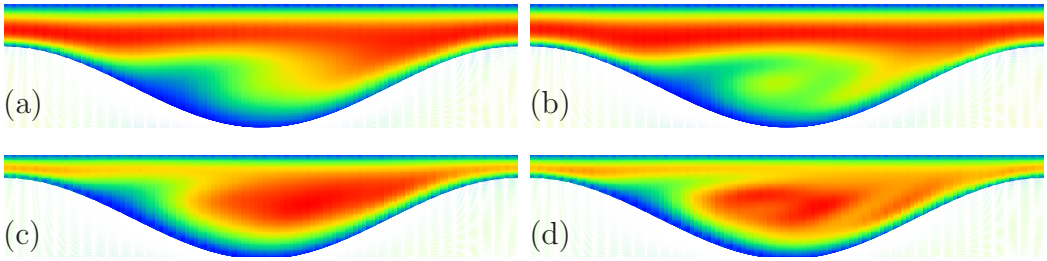

Fig. B.1. Resultant temperature field for the case of a lower plate with amplitude $a = 1/2$ and mean plate separations of $h = 1$ for (a) and (b), and $h = 3/4$ for (c) and (d): Peclét number $Pe = 300$ (left); $Pe = 1000$ (right).

which correspond to a constant temperature T_0 on both upper and lower plate.

Equation (B.2) is solved semi–analytically subject to the above boundary conditions using the Ritz direct method described in Section 3.1.2. Once again, a nonlocal variational formulation is employed, the corresponding functional of which is given by adding the term

$$-\left[T(-x,z)+T(x,z)\right]\left[4\left(\frac{\partial u}{\partial x}\right)^2+\left(\frac{\partial u}{\partial z}+\frac{\partial w}{\partial x}\right)^2\right], \tag{B.5}$$

to the integrand in equation (36). Subsequent steps are performed in full accordance with the procedure described in Section 3.1.2. Skipping such detail, the predicted temperature fields due to viscous heating for a lower plate with amplitude $a = 1/2$ and mean plate separations of $h = 1$ and $h = 3/4$ for two different Peclét numbers are shown in Figure B.1. In each case it is apparent that due to convection the dissipation heat is effectively spread throughout the flow domain, rather than remaining in the region where it is mainly produced, namely in the vicinity of the small gap where the local plate distance has a minimum and where the velocity gradient has a maximum. For a Peclét number of 1000, Figure B.1(b) and (d), the temperature maximum is actually found to lie inside the eddy far away from the narrowest point between the plates. Because of this very efficient spreading of dissipation heat, it is only to be expected that effects due to viscous heating should be negligible compared to those due to the imposed vertical temperature gradient: this can be verified as follows.

By considering both the temperature difference $T_1 - T_0$ between lower and upper plate and dissipation in combination, the resulting temperature field is given by superposition according to

$$T_{combined} = T + PrEcT^*, \tag{B.6}$$

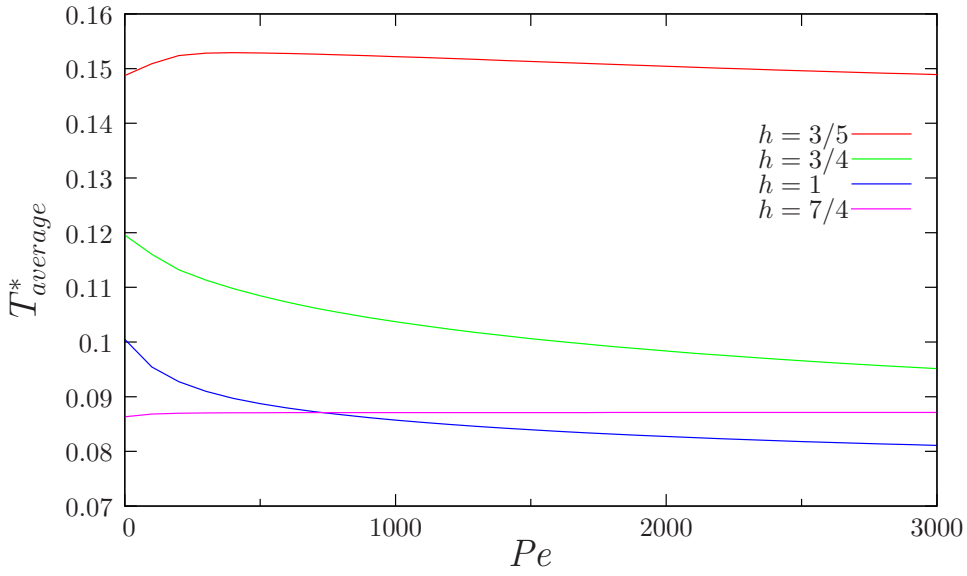

Fig. B.2. Profiles of averaged temperature, $T^*_{average}$ vs. Peclét number for the case of a flow geometry with a lower plate amplitude of $a = 1/2$, for four different mean plate separations, $h = 3/5$, $3/4$, 1, $7/4$.

with the temperature T being that resulting from the analysis given in Section 3.1.2. A rough estimate of the importance of the second term in (B.6) can be obtained by calculating the area averaged value of T^* for the case of a lower plate with amplitude $a = 1/2$, four different mean plate separations $h = 3/5$, $3/4$, 1, $7/4$, and various Peclét numbers; the results of which are plotted in Figure B.2. In all cases, $T^*_{average}$ is less than 0.2 and hence for a small dimensionless number $PrEc \ll 1$ dissipation effects are negligible, as expected.

Note that in the above verification the effect of the dissipation heat produced on the viscosity is not considered. In practice, such feedback would lead to a reduction in the viscosity and consequently to a reduction of dissipation heat; meaning that the effect of the latter would in fact be even smaller. Accordingly, the argument presented above can be thought of as a 'worst case estimation' for neglecting, as is done throughout the paper, the influence of dissipation.

References

Anthony, K.-H., 2001. Hamilton's action principle and thermodynamics of irreversible processes — a unifying procedure for reversible and irreversible processes. J. Non–Newtonian Fluid Mech. 96, 291–339.

Bateman, H., 1931. On dissipative systems and related variational principles. Phys. Rev. 38, 815–819.

Chandrasekhar, S., 1981. Hydrodynamic and Hydromagnetic Stability. Dover publications inc., New York.

COMSOL, 2005. Comsol multiphysics user guide v3.2.

Deuflhar, P., 1974. Modified newton method for solution of ill–conditioned systems of nonlinear equations with application to multiple shooting. Numerische Mathematik 22, 289–315.

Dowson, D., Higginson, G. R., 1966. Elastohydrodynamic lubrication. The fundamentals of roller and gear lubrication. Pergamon.

Etsion, I., 2005. State of the art in laser surface texturing. J. Rheology 127, 248–253.

Gaskell, P. H., Kapur, N., Savage, M. D., 2001. Bead–break instability. Phys Fluids 13(5), 1243–1253.

Gaskell, P. H., Savage, M. D., Wilson, M., 1997. Stokes flow in a half–filled annulus between rotating coaxial cylinders. J. Fluid Mech. 337, 263–282.

Jeffrey, D. J., Sherwood, J. D., 1980. Streamline patterns and eddies in low reynolds–number flow. J. Fluid Mech. 96, pp 315.

Jin, Z. M., Stone, M., Ingham, E., Fisher, J., 2006. Biotribology. Current Orthopaedics 20, 32–40.

Kistler, S. F., Schweitzer, P. M. (Eds.), 1997. Chapman & Hall, London.

Lide, D. R., 1998. CRC Handbook of Chemistry and Physics, 79^{th} Edition. CRC Press LLC.

Malevich, A. E., Mityushev, V. V., Adler, P. M., 2008. Couette flow in channels with wavy walls. Acta Mech. 197, 247–283.

Maple, 2006. Registered trademark of waterloo inc.

Panton, R. L., 1996. Incompressible Flow. John Wiley & Sons, Inc.

Perry, A. E., Chang, M. S., 1987. A description of eddy motions and flow patterns using critical–point–concepts. Ann. Rev. Fluid Mech. 18, pp 125.

Pozrikidis, C., 1987. Creeping flow in two–dimensional channels. J. Fluid Mech. 180, 495–514.

Reynolds, O., 1886. On the theory of lubrication and its application to mr. tower's experiments. Phil. Trans. R. Soc. Lond. 177, 159–209.

Sahlin, F., Glavatskih, S. B., Almqvist, T., Larson, R., 2005. Two–dimensional cfd–analysis of micro–patterned surface in hydrodynamic lubrication. Trans. ASME 127, 96–102.

Scholle, M., 2004. Creeping couette flow over an undulated plate. Arch. Appl. Mech. 73, 823–840.

Scholle, M., 2007. Hydrodynamical modelling of lubricant friction between rough surfaces. Tribology International 40, 1004–1011.

Scholle, M., Rund, A., Aksel, N., 2006. Drag reduction and improvement of material transport in creeping films. Arch. Appl. Mech. 75, 93–112.

Scholle, M., Wierschem, A., Aksel, N., 2004. Creeping films with vortices over strongly undulated bottoms. Acta Mech. 168, 167–193.

Serifi, K., Malamataris, N. A., Bontozoglou, B., 2004. Transient flow and heat transfer phenomena in inclined wavy films. IJTS 43, 761–767.

Sievers, B., Anthony, K.-H., 1996. Nonlocal lagrange formalism in the thermodynamics of irreversible processes: variational procedures for kinetic equations. Physica A 225, 89–128.

Spurk, J. H., Aksel, N., 2008. Fluid Mechanics. Springer.

Szeri, A. Z., 1998. Fluid Film Lubrication: Theory and Design. Cambridge University Press.

Tritton, D. J., 1988. Physical Fluid Dynamics, 2nd Edition. Oxford Science Publications, Clarendon Press, Oxford.

Tropea, C., Yarin, A. L., Foss, J. F., 2007. Handbook of Experimental Fluid Mechanics. Springer.

White, F., 2006. Viscous Flow. McGraw–Hill.

Wierschem, A., Scholle, M., Aksel, N., 2003. Vortices in film flow over strongly undulated bottom profiles at low reynolds numbers. Phys. Fluids 15, 426–435.

Wilson, M. C. T., Gaskell, P. H., Savage, M. D., 2005. Nested separatrices in simple shear flow: the effect of localised disturbances on stagnation lines. Phys. Fluids, 093601.

Zienkiewicz, O. C., Taylor, R. L., Zhu, J. Z., 2005. The Finite Element Method: Its Basis and Fundamental, 6^{th} Edition. Elsevier.